RSC Advances

PAPER

View Article Online
View Journal | View Issue

Cite this: *RSC Adv.*, 2024, **14**, 40006

Optimization of physicochemical properties of theophylline by forming cocrystals with amino acids†

Qi Li, ‡[a] Yifei Xie,‡[b] Zhipeng Wang,[a] Shuang Li,[a] Shiying Yang,[a] Dezhi Yang, *[a] Li Zhang,*[a] Guanhua Du[b] and Yang Lu*[a]

Received 21st September 2024
Accepted 15th December 2024

DOI: 10.1039/d4ra06804a

rsc.li/rsc-advances

This study presents the synthesis and characterization of novel cocrystal structures of theophylline (**THE**) with the amino acids gamma-aminobutyric acid (**GABA**) and L-arginine (**ARG**). Despite a large number of reports about **THE** cocrystals, no crystallographic parameters of cocrystals formed by **THE** and amino acids have been reported. **THE** is characterized by low solubility, while amino acids as cocrystal co-formers (CCFs) are increasingly recognized for their high solubility and safety. Consequently, the synthesis of cocrystals with amino acids has garnered considerable research interest. To optimize **THE**'s physicochemical properties, amino acids were chosen as CCFs, resulting in the synthesis of two novel cocrystals: **THE-GABA** and **THE-ARG-2H$_2$O**. Comprehensive characterization, such as X-ray diffraction analysis, spectral analysis, thermal analysis, and dynamic vapor sorption were conducted for **THE-GABA** and **THE-ARG-2H$_2$O**, alongside stability and solubility assessments. To better explain the characterization and evaluation results, the theoretical calculation methods were adopted, including the molecular electrostatic potential (MESP), topological analysis, energy framework, Hirshfeld surface and crystal voids. The study's findings reveal that the solubility and permeability of **THE** in both novel cocrystals, **THE-GABA** and **THE-ARG-2H$_2$O**, have increased, especially in the latter. Meanwhile, the hygroscopicity of them was at a low level which was basically consistent with **THE**.

Introduction

Theophylline (**THE**), a medication commonly used for respiratory diseases[1–3] like chronic obstructive pulmonary disease (COPD) and asthma,[1,2,4–7] functions by inhibiting phosphodiesterase (PDE) and thus preventing the breakdown of cAMP within cells. At least four anhydrous forms (form I, form II, form III, form IV) and a monohydrate of **THE** have been reported, among which form II is used for experiments. As a marketed form, form II is more stable than form I at room temperature.[8] Form III is produced by dehydration of monohydrate under low pressure or vacuum conditions.[9] Form IV is the most thermodynamically stable anhydrous polymorph.[10]

However, **THE** is associated with side effects like those of caffeine, primarily affecting the gastrointestinal system, such as nausea, as well as the psychiatric and nervous systems, including symptoms like anxiety and insomnia.[11,12] Furthermore, **THE**'s low water solubility restricts its pharmaceutical development and efficacy. Enhancing solubility can reduce the amount of active pharmaceutical ingredient (API) required for equivalent therapeutic effects.[13,14] Therefore, increasing the water solubility of **THE** has been a significant focus of research.

Cocrystals offer a promising method for enhancing the physical and chemical attributes of API.[15–17] Cocrystals are unique single crystals formed in a specific stoichiometric ratio, consisting of two or more distinct solid molecular compounds bonded through supramolecular forces.[17,18] In the context of APIs, incorporating cocrystal co-formers (CCFs) significantly alters the charge density of the molecule.[19,20] This development of cocrystals is often associated with modifications in their physicochemical properties.[21–24] Studies have demonstrated that cocrystals can alter various characteristics such as melting point, dissolution rate, thermal stability, and permeability, thereby impacting the drug's bioavailability without altering its chemical structure.[25]

Based on the Cambridge Crystallographic Data Centre (CCDC) and literature research, approximately 130 cocrystals of **THE** have been reported. One part of CCFs is acidic with an acidic group such as tartaric acid,[26] ferulic acid,[27] and aspirin.[28–30] The other part is nitrogen-containing alkaline, such

[a]*Beijing City Key Laboratory of Polymorphic Drugs, Center of Pharmaceutical Polymorphs, Institute of Materia Medica, Chinese Academy of Medical Sciences and Peking Union Medical College, Beijing 100050, P.R. China. E-mail: ydz@imm.ac.cn*

[b]*Beijing City Key Laboratory of Drug Target and Screening Research, National Center for Pharmaceutical Screening, Institute of Materia Medica, Chinese Academy of Medical Sciences and Peking Union Medical College, Beijing 100050, P.R. China*

† Electronic supplementary information (ESI) available. CCDC 2307422 and 2307423. For ESI and crystallographic data in CIF or other electronic format see DOI: https://doi.org/10.1039/d4ra06804a

‡ Qi Li and Yifei Xie contributed to the work equally as joint first authors.

as benzamide,[31] lamotrigine,[32] and niclosamide.[33–35] However, no crystals of **THE** with amino acids are reported on CCDC.

Amino acids, due to their low toxicity and natural occurrence, are deemed ideal and promising CCF candidates.[36] As zwitterions, amino acids can exhibit both acidity and alkalinity.[37] At the same time, amino acids have been widely used as CCFs to improve the stability and solubility of an API[38,39] in cocrystal structures. The solubility of ritonavir increased after forming a cocrystal with D-alanine.[40] In addition, cocrystals with amino acids can also reduce the side effects of the drug substance.[41] Mesalamine was an anti-inflammatory drug in the small intestine with a bloating effect. Mesalamine hydrochloride's cocrystal with glutamine had an acid–base stabilization effect in the gastrointestinal fluid, which reduced bloating.[42] There have been even cocrystals with amino acids already on the market, such as Steglatro (co-crystal between ertugliflozin and L-pyroglutamic acid) and Suglat (co-crystal between ipragliflozin and L-proline).[43] The commercially available product related to amino acids is sodium theophylline glycinate salt,[44] for which no crystallographic parameters have been reported. The sodium theophylline salt has been found to sustain high plasma concentrations of **THE** without posing a significant risk of severe adverse reactions.[45] This potential advantage highlights the substantial research significance of cocrystals formed by **THE** and amino acids.

Two novel cocrystals formed from **THE** and amino acids were obtained: theophylline-gamma-aminobutyric acid (**THE-GABA**) and theophylline-arginine-2H_2O (**THE-ARG-2H_2O**). The structures of API and CCFs are shown in Scheme 1. As illustrated in Scheme 2, the MESP of these compounds are marked by red areas indicating electron-rich regions and blue areas denoting electron-deficient regions. During the formation of zwitterionic ions *via* intramolecular proton transfer, the electron density tends to concentrate, which manifests itself in MESP as greater local maxima and smaller local minima. In this context, the electron-rich region of **THE** (carbonyl) has the potential to establish hydrogen bonds with the electron-deficient region (quaternary ammonium salt) of **GABA** and **ARG**.

In addition to its ability to cross the blood–brain barrier as a major inhibitory neurotransmitter in the mammalian central nervous system (CNS), gamma-aminobutyric acid (**GABA**) plays

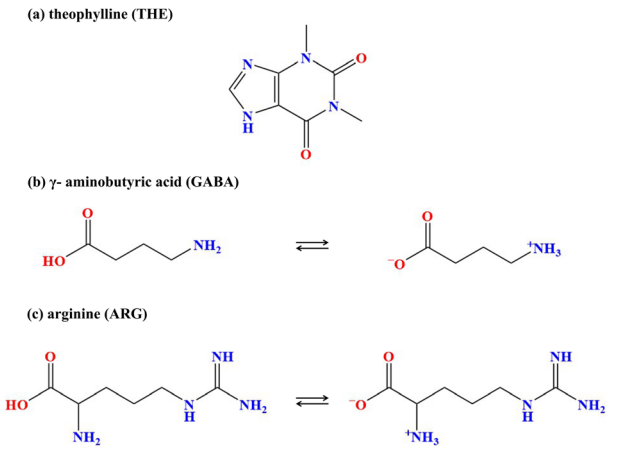

Scheme 1 Chemical structures of THE, ARG, and GABA.

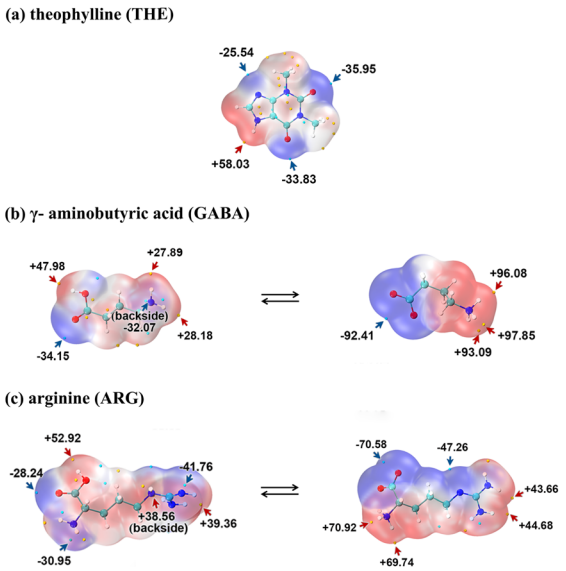

Scheme 2 MESP (kcal mol^{-1}) of THE, ARG, and GABA.

a crucial role in promoting neuronal development and relaxation, as well as in the prevention of insomnia and depression.[46,47] Arginine (**ARG**), classified as a nonessential amino acid in healthy adults,[48] contributes to immune function by increasing growth hormone secretion.[49] Therefore, the cocrystals of **THE-GABA** and **THE-ARG-2H_2O** hold promising implications in both pharmaceutical and nutritional domains.

In this study, the novel *de novo* synthesized cocrystals were characterized by single-crystal X-ray diffraction (SCXRD), powder X-ray diffraction (PXRD), differential scanning calorimetry (DSC), dynamic vapor sorption (DVS), and infrared spectroscopy (IR). Additionally, their solubility was systemically assessed in conditions simulating the *in vivo* environment and in pure water. Subsequently, the results were analyzed and interpreted through theoretical calculations.

Experiment

Materials

THE (Form II) raw material was purchased from Wuhan Yuancheng Gongchuang Technology Co., Ltd (Hubei, China). Arginine was acquired from Hubei Wande Chemical Industry Co., Ltd (Hubei, China), and γ-aminobutyric acid was obtained from Beijing Chemical Reagent Co. (Beijing, China). All analytical grade solvents were sourced from Sigma-Aldrich (St. Louis, MO, USA).

Synthesis and crystallization

Cocrystals of **THE-GABA** and **THE-ARG-2H_2O** were synthesized by solvent-assisted grinding with mortar and pestle. Equimolar amounts of **THE** (180.1 mg, 1 mmol) and **GABA** (103.1 mg, 1 mmol) with 4 mL ethanol were ground for about 40 min and equimolar amounts of **THE** (180.1 mg, 1 mmol) and **ARG** (174.2 mg, 1 mmol) in 2 mL water were ground for about 40 min. The two cocrystals were both dissolved in methanol and then left to stand under ambient conditions for approximately 5–10 days, resulting in the formation of colorless crystals.

Unsaturated states of **THE**: to attain unsaturation, 2 mL water solution was added, followed by approximately 10 mg of **THE**. The solution was stirred at 37 °C for 48 hours after the rotor was added, and the residual powder was measured after the water solution evaporated.

Supersaturated states of **THE**: to attain supersaturation, 2 mL water solution was added, followed by approximately 50 mg of **THE**. The solution was stirred at 37 °C for 48 hours after the rotor was added, and the residual powder was measured after the water solution evaporated.

SCXRD analysis

The Rigaku XtaLAB Synergy four-circle diffractometer (Rigaku, Americas) with Cu-Kα radiation ($w\lambda = 1.54178$ Å) was used to collect all the diffraction intensity data of single crystals. The SCXRD measurement was conducted at 293 K. Crystal structures were generated through Olex2 (Version 1.5)[50–53] and SHELXL (2018.3)[54] software. The crystal structure was solved by the direct method,[55] using the least squares method to correct the structural parameters. All the non-hydrogen atoms were refined anisotropically and the hydrogen atoms were located using Fourier analysis and geometric calculation.

THE-GABA (1 : 1) crystallized in the *Ia* space group of the monoclinic system and the asymmetric unit of one contains one **THE** molecule and one **GABA** molecule. **THE-ARG-2H$_2$O** (1 : 1 : 2) crystallized in the *P*1 space group of the triclinic system and the asymmetric unit of one contains one **THE** molecule, one **ARG** molecule and two water molecules.

PXRD analysis

PXRD patterns of API, CCFs, and cocrystals were collected with a Rigaku D/Max-2550 powder X-ray diffractometer (Rigaku, Tokyo, Japan) under a Cu Kα radiation of $\lambda = 1.54178$ Å, 2θ scanning range of 3–40°, and a scanning speed of 8° min^{-1}. Simultaneously, the theoretical powder patterns of the cocrystals were calculated using the Mercury (Version 2023.3.0)[56] software.

DSC analysis

DSC curves of API, CCFs, and cocrystals were measured by a DSC instrument (Mettler Toledo, Switzerland). Samples (3–5 mg) were placed in an aluminum crucible with a lid and heated at 10 °C min^{-1}. STARe evaluation software (Version 16.30) was used to process the atlas.

IR analysis

Each sample was measured by Spectrum 400 Fourier transform IR with attenuated total reflection accessory (PerkinElmer, Waltham, MA, USA). The experimental conditions were over the range of 4000–400 cm^{-1} with 16 scanning times having a resolution of 4.000 cm^{-1}.

DVS analysis

DVS is a well-established method for the measurements of vapor sorption and desorption.[57,58] Surface Measurement Systems (SMS) DVS apparatus (London, U.K.) was used to record moisture sorption and desorption measurements of **THE** and cocrystals. Approximately 30–50 mg of the sample was placed onto a quartz DVS round-bottom pan. The sample was pre-equilibrated with a continuous flow of dry nitrogen for 5 min. Subsequently, the relative humidity (RH) was incrementally increased from 0% to 90%, with each step consisting of a 10% increase. Following this, the RH gradually decreased to 0% in equal increments. Throughout the process, the equilibrium criterion, defined as d_m/d_t (the rate of mass change over time), was maintained at 0.02% min^{-1} for every step.

Solubility measurements

The solubility tests of **THE** and cocrystals were performed at 37 °C in the dissolution media of water (pH 7.0), phosphate buffer (pH 6.8), acetate buffer (pH 4.5), and hydrochloric aqueous solution (pH 1.2). The buffer recipes were as follows: pH 7.0: purified water; pH 6.8 : 6.8 g of potassium dihydrogen phosphate and 0.94 g sodium hydroxide were dissolved in 1 L water; pH 4.5 : 18 g sodium acetate and 9.8 mL glacial acetic acid were added to 1 L water; pH 1.2 : 9 mL hydrochloric acid was added to 1 L water.

After the addition of 2 mL buffer solution, about 50 mg cocrystal samples were added to achieve a suspension state. Subsequently, the mixture was stirred for 48 h at 37 °C, diluted to the desired concentration, and analyzed using high-performance liquid chromatography (HPLC). The concentrations of **THE** were quantified on an Agilent HPLC system (Agilent 1200 series, East Brunswick, NJ, USA) with a Welch Materials XB-C18 column (4.6 mm × 250 mm, 5 μm), and the detection wavelength was 271 nm. The mobile phase was prepared with water: ACN (85 : 15); the flow rate was 1 mL min^{-1}, and the column temperature was set at 30 °C. The remaining powder was collected and dried for phase analysis by PXRD.

IDR test

The intrinsic dissolution rate (IDR) of **THE** and its cocrystals was measured by an RC12AD dissolution apparatus over 30 min. Accurately weighed solids equivalent to 120 mg of **THE** were placed in the intrinsic attachment and compressed at a pressure of 300 kg for 1 min to create a flat surface on one side. The container holding the compressed sample was immersed in 900 mL of deionized water, maintained at a temperature of 37 ± 0.2 °C. Samples were collected at 2, 6, 10, 14, 18, 22, 26, 30 min at 37 °C and 100 rpm rotating speed at the same depth. After filtration through a 0.45 μm syringe tip filter, the samples were detected on an HPLC system while the test condition remained the same as mentioned in Solubility measurements.

Permeability test

Permeability of **THE** and cocrystals was determined experimentally by cellulose nitrate membrane (0.45 μm, Cytiva, Germany) and a modified Franz diffusion cell apparatus. 5 mL buffer medium (pH 6.8) was added to the device and bubbles were expelled. The buffer medium was then kept at 37 ± 0.2 °C

and rotated at 100 ± 5 rpm. Then 10 mg **THE** and the same equivalent of cocrystals were placed on the membrane. According to the set predetermined time, a 0.5 mL sample was taken from the device at a time and supplemented with fresh medium.

Theoretical calculation

The intermolecular interactions between API and CCFs were explored by density functional theory, and topological analysis was conducted by applying the quantum theory of atoms in molecules (QTAIMs).[59] The B3LYP-D3/6-31G* level was employed for all the hydrogen atom geometry optimizations. The B3LYP-D3/6-311G** level was used for single point energy calculations using Gaussian 16 package.[60] The Multiwfn 3.8 program was used for all wave function analyses.[61] Crystal voids, promolecule density, and energy frameworks were calculated using CrystalExplorer 21.3 software.[62]

Results and discussion

Crystal structure analysis

The two cocrystals obtained by the slow evaporation method were characterized by SCXRD. The detailed crystallographic information on all cocrystals is listed in Table 1. Hydrogen bond interactions are the main motivations for the formation of these cocrystals. The detailed formation of hydrogen bonds is listed in Table S1.† The formation of hydrogen bonds is accompanied by changes in electron density around atoms close to each other. The electron density around different hydrogen bond motifs is partially shown in Fig. 3. Besides, the cocrystal lattice energies already reported for **THE** were summarized (Fig. S1†). The two cocrystal lattice energies are in average positions. The cocrystals of **THE** involved in Fig. S1 are listed in Table S2.†

In **THE-GABA**, the main hydrogen bond motifs are shown on the left of (a) in Fig. 1. The hydrogen bonds of N_4–$H_4\cdots O_{1S}$ (2.68 Å) and N_{1S}–$H_{1S}\cdots N_3$ (3.09 Å) link the **THE** and **GABA** molecules together. The oxygen atoms of the carboxylate group of the **GABA** molecule act as H-bond acceptors towards **THE** molecule (O_{1S}) and two **GABA** molecules (O_{2S}, which works as bifurcated acceptors), as shown in Fig. 1. These hydrogen bond interactions assemble **THE** and **GABA** molecules. Besides, the two planes where **THE** and **GABA** are located separately form 66° in Fig. 2.

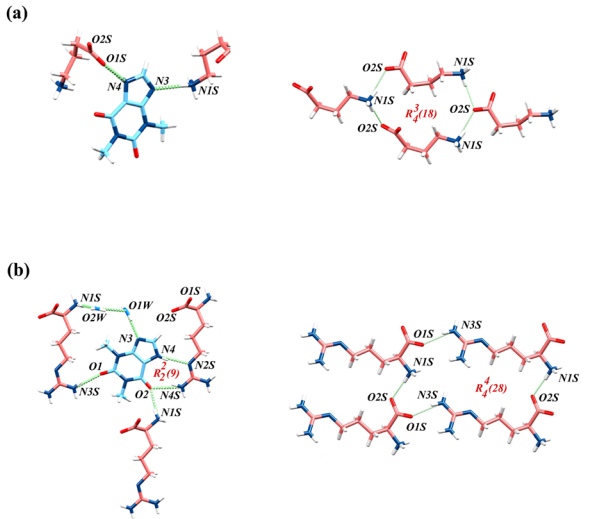

Fig. 1 (a) Hydrogen bonding interactions and hydrogen bond motifs $R_4^3(18)$ of THE-GABA; (b) Hydrogen bonding interactions and hydrogen bond motifs $R_2^2(9)$ and $R_4^4(28)$ of THE-ARG-2H_2O.

In **THE-ARG-2H_2O**, the hydrogen bonds are -affected by the presence of two water molecules. N_3 of **THE** forms a hydrogen bond with O_{1W}–H_{1WB} of one water molecule, which forms a hydrogen bond with O_{2W} of another water molecule at the same time. And O_{2W} forms a hydrogen bond with N_{1S} of **ARG**. The hydrogen bond interactions connect **THE**, **ARG** and two water molecules. Water in organic molecules can be divided into two categories: lattice water and channel water. Fig. S2† illustrates the analysis of the locations of crystallization water molecules, conducted using the water analyzer module of Mercury. And the water in **THE-ARG-2H_2O** belongs to channel water. The probe radius is set to 1.2 Å, which is the approximate molecular radius of one water molecule. The volume of the water molecule is 53.80 Å^3, which is 11.7% of unit cell volume. Similar to **THE-GABA**, the hydrogen bond is formed by the carboxyl group and the amino group of **ARG** molecules. However, the connection of the amino group of **ARG** to **THE** is

Table 1 Crystal cell parameters and structure refinement of the cocrystals

Cocrystal		
Formula	**THE-GABA**	**THE-ARG-2H_2O**
Space group	*Ia*	*P*1
a (Å)	7.2517(2)	5.8709(2)
b (Å)	21.6583(5)	7.7140(3)
c (Å)	8.7412(3)	11.1553(3)
α (deg.)	90	72.564(3)
β (deg.)	112.434(3)	81.718(3)
γ (deg.)	90	72.804(3)
Volume (Å^3)	1268.99(7)	459.59(3)
Z	4	1
Density (g cm^{-3})	1.483	1.411
R_1 ($I > 2\sigma(I)$)	0.0416	0.0430
wR_2 ($I > 3\sigma(I)$)	0.1127	0.1155
CCDC deposition no.	2307422	2307423

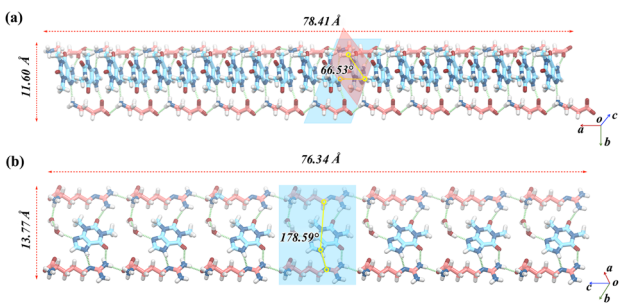

Fig. 2 (a) The stepped-like structure of THE-GABA; (b) the ladder-like structure of THE-ARG-2H_2O.

assisted by two water molecules. Unlike **THE-GABA**, the carbonyl groups in **THE** are involved in forming classical hydrogen bonds.[63,64] "Classical hydrogen bond" refers to hydrogen bonds that donors do not include groups consisting of C–H. **THE** is connected with one **ARG** by N_4–H_4⋯N_{2S} and N_{4S}–H_{4S}⋯O_2 in the motif $R_2^2(9)$. Hydrogen bonds N_{3S}–H_{3S}⋯O_1 and O_{1W}–H_{1W}⋯N_3 are also involved in the connection of **THE** and **ARG**. Furthermore, because **THE**, **ARG**, and the two water molecules are almost on the same plane (178.59°), the hydrogen bond interactions assemble them into a ladder-like structure, as shown in the middle of (b) in Fig. 2. From the ladder structure, the hydrogen bonds between the two water molecules significantly contribute to stabilizing **THE**'s binding to the chain structure formed by **ARG**.[65,66]

Topological analysis

Topological analysis based on atoms in molecules (AIM) theory can be used to analyze hydrogen bond relationships, in which bond critical point (BCP) and bond path are important parameters. For classical hydrogen bonds, hydrogen bond strength is the focus in the study of intermolecular interactions to distinguish the strength of interactions. Sometimes, bond path length is used to compare the strength of hydrogen bonds, but it is an unreliable criterion for judgment. According to,[67] the electron density at BCP has an optimal correlation with the strength of hydrogen bonds. This study uses this method to analyze the strength of each hydrogen bond formed with **THE** in each cocrystal while comparing it to the bond path length. The results are shown in Fig. 3. For example, in cocrystal **THE-ARG-2H$_2$O**, imidazole in **THE** forms a hydrogen bond with the guanidine group in **ARG** with a bond path length of 2.915 Å, which is supposed to be a weak hydrogen bond as judged from the bond path length. However, the results show that this hydrogen bond is the strongest in Fig. 3(b) because of the highest electron density at BCP.

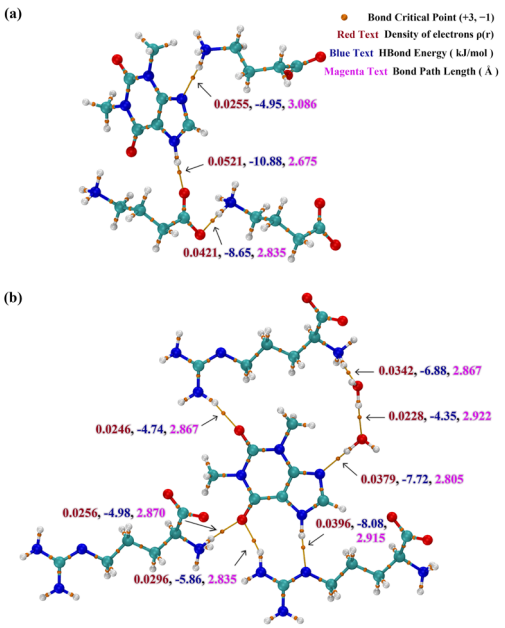

Fig. 3 Topological analysis of the electronic density of THE-GABA (a) and THE-ARG-2H$_2$O (b).

PXRD analysis

PXRD is mainly used for the solid-phase analysis of powder.[68] The newly formed cocrystals often have specific PXRD patterns due to their unique crystal structure. Therefore, PXRD patterns of the cocrystal are compared with patterns calculated from the SCXRD structure (Fig. 4: left). To facilitate intuitive observation of the variation of the diffraction peaks, the variation in the characteristic diffraction peaks is labeled as "★". The pure phase of API and CCFs PXRD patterns are included. It is evident that the patterns calculated from the SCXRD structure (labeled with the prefix "THEO") align closely with the experimental patterns. Notably, the primary characteristic peaks of **THE** and CCFs disappear, and new characteristic diffraction peaks are generated, signifying the creation of new phases. Water molecules are presented in **THE-ARG-2H$_2$O**. The removal of water molecules at elevated temperatures was conducted to determine the feasibility of obtaining anhydrous **THE–ARG**. Upon equilibrating the powder of **THE-ARG-2H$_2$O** at 130 °C for 30 minutes, the PXRD pattern of the powder exhibited peaks corresponding to **THE** and **ARG**. The anhydrous **THE–ARG** was ultimately not acquired.

Thermal analysis

DSC is a common detection technique to identify thermodynamic changes in cocrystal and crystalline forms.[69] The DSC curves of cocrystals are shown in Fig. 4 (right). **THE-GABA** exhibited a melting endothermic peak at 232.25 °C, whereas **THE-ARG-2H$_2$O** showed a corresponding peak at 133.98 °C. Among them, the endothermic peak of **THE-ARG-2H$_2$O** at 133.98 °C indicates the release of water, and then melting occurs after 190 °C. The peaks of the cocrystal exhibit apparent differences from API or CCFs, which implies the formation of cocrystals. TG (Fig. S3:† right) analysis was applied to investigate the crystalline solvent presented in the structures. Therefore, based on the results of TG analysis, the cocrystal **THE-**

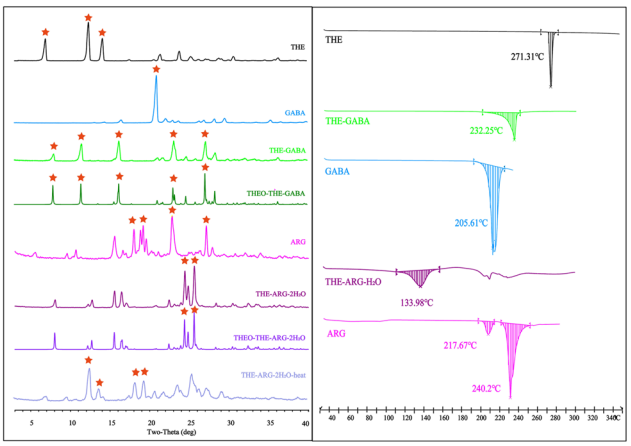

Fig. 4 PXRD patterns (left) and DSC (right) of API, CCFs, and the corresponding cocrystals (characteristic peaks are marked as ★).

GABA does not contain solvent or water. For **THE-ARG-2H$_2$O**, the TG curve shows a weight loss step in the temperature range of 80–140 °C, and the mass loss rate is 8.68%, consistent with the theoretical mass loss rate of 9.23% of two water molecules.

IR analysis

The formation of the hydrogen bonding interaction between API and CCFs led to changes in the IR spectra of the cocrystals compared with the IR spectra of API and CCFs.[70] SCXRD data show that the sites forming hydrogen bonds of **THE** mainly are on the secondary amine and imine group of the imidazole ring and carbonyl of the pyrimidine ring. The intermolecular hydrogen bonding interaction led to alterations in the IR spectra of the cocrystals, specifically in the wavenumber bands of 3500–3100 cm^{-1} (ν_{N-H}), 3400–3300 cm^{-1} ($\nu_{C=N}$) and 1690–1640 cm^{-1} ($\nu_{C=O}$). Compared with **THE**, the cocrystals of vibration frequency generally moved to lower frequencies. The main vibrational data of the cocrystals and their preliminary attribution are shown in Table S3, and the IR spectra are shown in Fig. S3 (left).†

DVS analysis

Hygroscopicity can be defined as "a phenomenon that occurs when a certain amount of water vapor exposed to a solid at a given temperature and relative humidity is taken up and retained utilizing noncovalent interactions, particularly hydrogen bonding, with some effect on the surface and/or bulk properties of the solid".[71,72] Hygroscopicity may be attributed to the forming of hydrogen bonds between functional groups exposed to air on a solid surface and water molecules and voids in the crystal structure.[73] **ARG** and **GABA** as zwitterions (Schemes 1 and 2) can cause strong ion–water interaction, so the hygroscopic properties of API, amino acid, and cocrystals were examined.

Sorption and desorption of **THE**, **GABA**, **ARG**, and their cocrystals are illustrated in Fig. S4.† The results from the DVS indicate that the anhydrous forms of **THE** (BAPLOT01) and **ARG** (ARGIND11) exhibit negligible hygroscopicity, with values of 0.075% and 0.786%, respectively. In contrast, **GABA** (GAMBUT01) displays significant hygroscopic characteristics, with a much higher value of 63.33%. Notably, the formed cocrystals reduce the hygroscopicity of **GABA** and **ARG** to varying degrees.

The hygroscopicity of **THE-GABA**, measured at 0.064%, falls below the standard threshold of 0.2% for hygroscopicity, categorizing it as having negligible or virtually no hygroscopic properties. Although the moisture weight gains of the **THE-ARG-2H$_2$O** (0.426%) are higher than that of **THE**, it only belongs to the substance with slight hygroscopicity. The crystal voids were examined (Fig. 5 and Table 2) about the potential presence of voids following the development of the co-crystals, which could let the ingress of water molecules, ultimately compromising the structure.

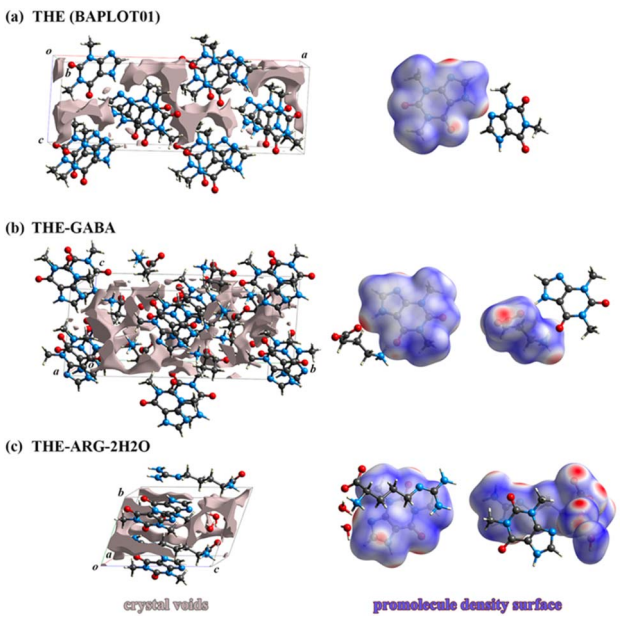

Fig. 5 Crystal voids occupied in the unit cell and promolecule density surface of THE (a), cocrystal THE-GABA (b), and THE-ARG-2H$_2$O (c) at a 0.002 a.u. isosurface.

Crystal voids analysis

The void space refers to the unoccupied areas within a crystal structure where solvent molecules can attach or be incorporated during dissolution or solvation processes. In a novel cocrystal complex of **THE** and malonic acid,[14] the hygroscopicity of **THE** and its cocrystals were linked to the voids and promolecule density[74] of the respective crystals. The relevant calculation results are listed in Table 2 and shown in Fig. 5. Generally, smaller voids or a higher promolecule density in the crystal correlate with reduced hygroscopicity. This correlation has been confirmed in the case of the **THE-GABA** cocrystal. However, the dihydrate cocrystal, **THE-ARG-2H$_2$O**, deviates from this pattern, likely due to the inherent water content of the hydrate itself.

Solubility and IDR

High solubility and fast dissolution are essential for optimal pharmacokinetics and improved therapeutic efficacy.[75]

Table 2 The information of the void surface and promolecule density (isovalue 0.002 e au^{-3})

Compounds	Voids (Å^3)	Voids (%)	Promolecule density (Å^3)	Promolecule density (%)	Moisture weight (%)
THE	79.80	10.0	174.24	87.0	0.0749
THE-GABA	76.98	6.1	291.79	92.1	0.0660
THE-ARG-2H$_2$O	44.82	9.8	412.43	89.7	0.428

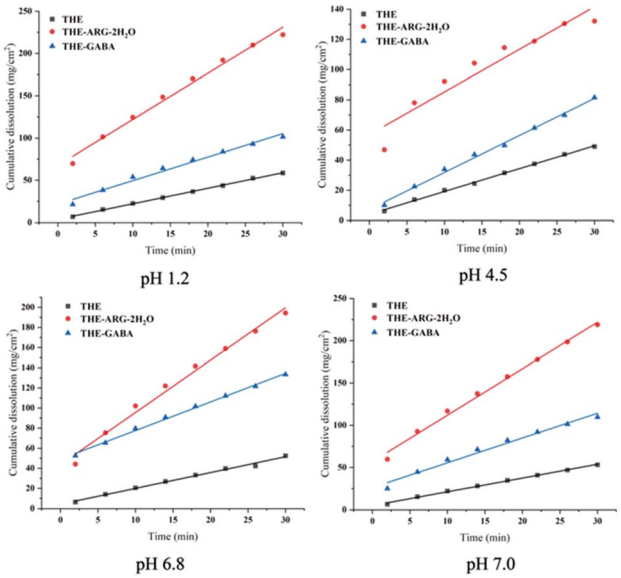

Fig. 6 IDR results of THE and cocrystals.

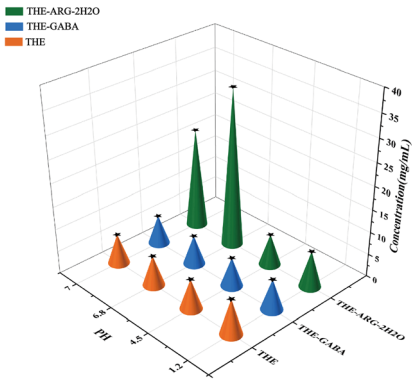

Fig. 7 Solubility results of THE and cocrystals.

The IDR parameter is a good indicator to predict bioavailability performance. The IDR results of **THE** cocrystals are presented in Fig. 6. At pH 7.0, 6.8, 4.5, and 1.2, **THE-ARG-2H$_2$O** and **THE-GABA** significantly increase the dissolution rate of **THE** in the order **THE-ARG-2H$_2$O** > **THE-GABA.**

Fig. 7 and Table 3 show the solubility, final solid powder and post-experimental pH results of **THE** (**THE** form II, CSD ref-code BAPLOT) at pH = 1.2, pH = 4.5, pH = 6.8, and pH = 7.0 buffered solutions. Solubility experiments were carried out by the suspension stirring method at 37 °C for 48 h. The solubilities of **THE-ARG-2H$_2$O** are higher than that of **THE** at pH = 6.8 and pH = 7.0 buffered solutions, around five times and 3.2 times, respectively. After the buffered solutions were absorbed, the final powder in the vial was subjected to PXRD testing. Interestingly, it was observed that only at pH levels of 7.0 and 6.8 did the PXRD patterns of the final powder closely match those of **THE-ARG-2H$_2$O**. In contrast, whether it is **THE-ARG-2H$_2$O** at pH 1.2 and pH 4.5, or **THE-GABA** and **THE** in the four buffered solutions, the final powder predominantly transforms into a monohydrate of **THE**. Concurrently, it is also noted that these powder patterns largely correspond with **THE** in supersaturated water. The pH was measured after the experiments. The PH values of **THE-GABA** and **THE** are close to each other in the four media solutions. In contrast, in **THE-ARG-2H$_2$O**, the data of pH in four media solutions are greater than **THE**, with 6.8 being close to 7.0. This may be because the pK_a value of **ARG** is greater than those of **GABA** and **THE**. The pH values in Table 3 suggest that the buffer capacity was overwhelmed in some cases. This is all the more reason to list the suspension composition in the Experiment section.

The process of solubility occurs when the cocrystals enter the aqueous solution, the crystal surface is surrounded by water molecules, which also enter the void space thereby structurally disintegrating. Since the molecules generally tend to exist in a more stable state, the more water-soluble CCF leaves the lattice first into the aqueous medium.[76] The results of IDR and solubility experiments show that the dissolution rate of **THE-GABA** is significantly improved compared to that of **THE**, but no change is notable in solubility. This may be because the presence of **GABA** could not limit the transformation of **THE** polymorph II to **THE** monohydrate during standing at equilibrium solubility. In **THE-ARG-2H$_2$O**, the guanidine group of **ARG** exhibits sensitivity to hydrogen ion concentration, indicating that pH (H^+ concentration) influences the state of the cocrystals, which exist in a cocrystal state at pH 6.8 and 7.0.

Furthermore, the conversion of **THE** polymorph II with water to **THE** monohydrate necessitated supersaturation conditions

Table 3 Solubility of THE and cocrystals (mean ± SD mg mL^{-1}, n = 3)

	Compound	**THE**	**THE-GABA**	**THE-ARG-2H$_2$O**
pH 1.2	Saturation concentration	7.8 ± 0.09	6.81 ± 0.06	8.05 ± 0.18
	Post-experimental pH	1.84	2.04	3.21
	Final solid powder	Monohydrate of **THE**	Monohydrate of **THE**	Monohydrate of **THE**
pH 4.5	Saturation concentration	6.67 ± 0.17	6.42 ± 0.58	6.95 ± 0.059
	Post-experimental pH	4.80	4.82	5.53
	Final solid powder	Monohydrate of **THE**	Monohydrate of **THE**	Monohydrate of **THE**
pH 6.8	Saturation concentration	6.68 ± 0.12	6.49 ± 0.04	34.83 ± 1.00
	Post-experimental pH	6.90	6.88	8.92
	Final solid powder	Monohydrate of **THE**	Monohydrate of **THE**	Cocrystal
pH 7.0	Saturation concentration	6.66 ± 0.31	6.42 ± 0.26	21.55 ± 2.09
	Post-experimental pH	6.27	6.28	8.93
	Final solid powder	Monohydrate of **THE**	Monohydrate of **THE**	Cocrystal

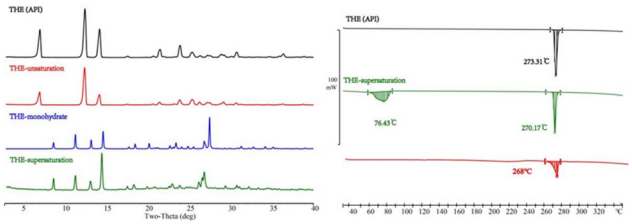

Fig. 8 PXRD and DSC patterns of THE.

that were discovered serendipitously. The supersaturated and unsaturated states of **THE** in water were compared. As observed in Fig. 8, it is found that under identical conditions in water, only the supersaturated state of **THE** (polymorph II) primarily converted into **THE** monohydrate. The PXRD pattern observed in the unsaturated state remains consistent with the API form of **THE**.

Permeability

Oral drug bioavailability is mainly affected by the permeability of drugs through the gastrointestinal membrane and the solubility/dissolution of drugs in the gastrointestinal environment.[1] Therefore, intestinal pH 6.8 was simulated to conduct permeability studies on **THE** and cocrystals. The results are shown in Fig. 9. Taking into account the importance of the apparent permeability coefficient (P_{app}) values for the overall evaluation of the permeability of drug-like compounds. The P_{app} of **THE** is 142.40 × 10^{-6} cm s^{-1}, the P_{app} of **THE-GABA** is 85.59 × 10^{-6} cm s^{-1}, and the P_{app} of **THE-ARG-2H$_2$O** is 31.32 × 10^{-6} cm s^{-1}. In Fig. 9, **THE-ARG-2H$_2$O** has basically reached saturation penetration at 60 min, **THE-GABA** has basically reached saturation at 180 min, and **THE** has not reached saturation after 250 min. Therefore, both cocrystals improve the permeability of **THE**, especially **THE-ARG-2H$_2$O**.

Hirshfeld surface and 3D energy frameworks

The nature and individual contributions of each intermolecular interaction within a crystal lattice can be illustrated by the Hirshfeld surface. The fingerprint on the right and percentage

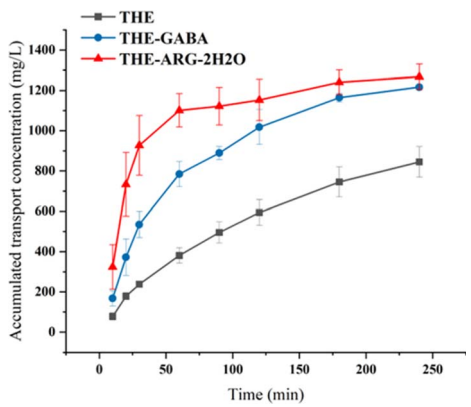

Fig. 9 Permeability results of THE and cocrystals.

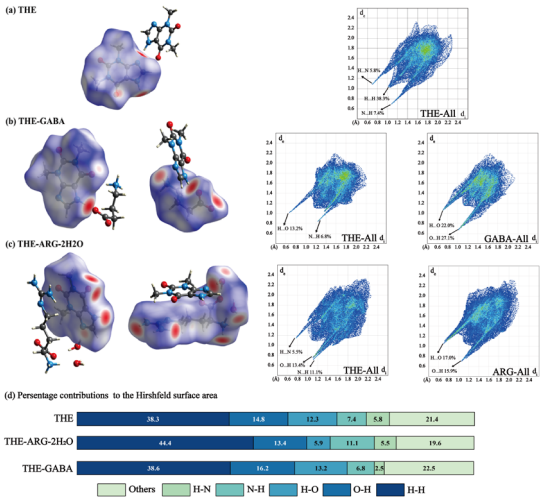

Fig. 10 Hirshfeld surface (mapped with d_{norm}) of THE (a), THE-GABA (b) and THE-ARG-2H$_2$O (c) and percentage contributions to the Hirshfeld surface area (d).

contributions to the Hirshfeld surface revealed that H···H contacts have maximum contributions in both cocrystals. In Fig. 10, the deep red spots indicate sites where hydrogen bonds were formed, and the shade of color corresponds to the strength of the interaction. In **THE-GABA**, O···H (16.2%), H···O (13.2%), and N···H (6.8%) interactions have high contributions to the Hirshfeld surface. In **THE-ARG-2H$_2$O**, O···H (13.4%), N···H (11.1%), and H···O (5.9%) interactions have notable contributions to the Hirshfeld surface. The H–O/O–H and N–H/H–N contributions of **THE**, **THE-GABA** and **THE-ARG-2H$_2$O** were 40.3%, 35.9%, and 38.7%, respectively.

The 3D energy framework can be utilized to analyze the energy interaction between molecules. This total interaction energy is calculated per unit cell. The energy framework calculations are based on molecular wave functions, generating electron densities using the CE-B3LYP/6-31G (d, p) method. The energy frameworks for the molecule, encompassing coulomb, dispersion, and total energies, are depicted using cylinders of different colors. These cylinders were scaled (tube size) by a factor of 100 and have a cut-off energy of −5 kJ mol^{-1}. The cylinder's diameter varies according to the strength of the interaction. As illustrated in Fig. S5,† the calculation results reveal that Coulomb energy predominates in **THE** and **THE-ARG-2H$_2$O**. However, dispersion energy is also significant in **THE** and **THE-ARG-2H$_2$O**. The relationship between Coulomb and dispersion energies is reversed in the **THE-GABA** cocrystal, with dispersion energy playing the leading role.

Conclusions

In this study, two novel cocrystals with amino acids were synthesized successfully, **THE-GABA** and **THE-ARG-2H$_2$O**, using solvent-assisted grinding and slow evaporation methods. To identify the predominant cocrystal form, a range of characterizations were conducted, including SCXRD, PXRD, DSC, TGA, and IR, as well as solubility, IDR, permeability and

hygroscopicity evaluations. Topological analysis, Hirshfeld surface and 3D energy frameworks were used to analyze intermolecular interaction forces and Crystal voids analysis was used to analyze hygroscopicity. Although **THE-GABA** demonstrates an enhancement in dissolution rate and permeability, **THE-ARG-2H$_2$O** displays a more pronounced rise. This may result from variations in the solubility of CCFs. In the Hirshfeld surface results, a smaller percentage of O–H/H–O and N–H/H–N, suggesting weaker intermolecular hydrogen bonding, may explain the higher solubility of **THE-ARG-2H$_2$O**. The solubility experiments indicated that the solubility of **THE-ARG-2H$_2$O** enhanced solely at pH levels 6.8 and 7.0. The guanidinium group of **ARG** is sensitive to hydrogen ion concentration, leading to minimal enhancement in solubility at pH 4.5 and 1.2. Consequently, APIs or CCFs with guanidine groups must consider the influence of pH during polymorphic or cocrystal activity. In addition, it was unexpectedly found that the conversion of **THE** polymorph II to **THE** monohydrate requires supersaturation conditions (water solution). Therefore, the saturation state of **THE** must be considered during pharmacological operations involving water solution related to **THE**. Our study provides experience and examples for exploring the structure–property relationships in pharmaceutical cocrystals. **THE-ARG-2H$_2$O**, as a superior cocrystal form, significantly enhances the solubility of **THE** while remaining stable, offering valuable material for further *in vivo* studies.

Data availability

The dates of the compounds are available from the authors.

Author contributions

Conceptualization, L. Z. and Y. L.; methodology, Q. L. and Y. X. software, D. Y. and S. L.; validation, D. Y., S. L. and Y. X.; formal analysis, Q. L. and Y. X.; investigation, Y. X. and Q. L.; resources, Q. L. and Z. W; data curation, Z. W. and Q. L; writing—original draft preparation, Q. L.; writing—review and editing, D. Y. and L. Z.; visualization, S. Y.; supervision, L. Z., D. Y. and Y. L.; project administration, G. D.; funding acquisition, Y. L., L. Z. and D. Y. All authors have read and agreed to the published version of the manuscript.

Conflicts of interest

There are no conflicts to declare.

Acknowledgements

This research was funded by the National Natural Science Foundation of China (Grant No. 22278443), CAMS Innovation Fund for Medical Sciences (Grant No. 2022-I2M-1-015), the Key R&D Program of Shan Dong Province (Grant No. 2021ZDSYS26), Chinese Pharmacopoeia Commission Drug Standard Promoting Fund (Grant No. 2023Y11), Independent Innovation and Achievement Transformation Plan Project of Zaozhuang City (Grant No. 2022GH15), the Xinjiang Uygur Autonomous Region Innovation Environment Construction Special Fund and Technology Innovation Base Construction Key Laboratory Open Project (Grant No. 2022D04016) and 2021 Tengzhou Talent Project.

References

1 P. J. Barnes, Theophylline, *Am. J. Respir. Crit. Care Med.*, 2013, **188**(8), 901–906.
2 M. Weinberger and L. Hendeles, Theophylline in asthma, *N. Engl. J. Med.*, 1996, **334**(21), 1380–1388.
3 K. F. Rabe, H. Magnussen and G. Dent, Theophylline and selective PDE inhibitors as bronchodilators and smooth muscle relaxants, *Eur. Respir. J.*, 1995, **8**(4), 637–642.
4 L. L. Gong, L. D. Du and G. H. Du, *Theophylline*, Natural Small Molecule Drugs from Plants Ch., 2018, vol. 78, pp. 469–474.
5 J. D. Journey and T. P. Bentley, *Theophylline toxicity*, StatPearls, 2018.
6 Y. Ma, D. Jiang, J. Meng, M. Li, H. Zhao, Y. Wang and L. Wang, Theophylline: a review of population pharmacokinetic analyses, *J. Clin. Pharm. Therapeut.*, 2016, **41**(6), 594–601.
7 J. B. Peter, Theophylline, *Am. J. Respir. Crit. Care Med.*, 2013, **188**(8), 1–19.
8 K. Fucke, G. J. McIntyre, C. Wilkinson, M. Henry, J. A. Howard and J. W. Steed, New insights into an old molecule: interaction energies of theophylline crystal forms, *Cryst. Growth Des.*, 2012, **12**(3), 1395–1401.
9 K. Matsuo and M. Matsuoka, Solid-state polymorphic transition of theophylline anhydrate and humidity effect, *Cryst. Growth Des.*, 2007, **7**(2), 411–415.
10 L. Seton, D. Khamar, I. J. Bradshaw and G. A. Hutcheon, Solid state forms of theophylline: presenting a new anhydrous polymorph, *Cryst. Growth Des.*, 2010, **10**(9), 3879–3886.
11 H. Leslie, W. Miles, S. Stanley and E. Elliot, Safety and efficacy of theophylline in children with asthma, *J. Pediatr.*, 1992, **120**(2), 177–183.
12 M. Weinberger and L. Hendeles, Therapeutic effect and dosing strategies for theophylline in the treatment of chronic asthma, *J. Allergy Clin. Immunol.*, 1986, **78**(4), 762–768.
13 L. P. Ji, R. M. Chang, Q. Q. Xu, J. J. Chen, S. F. Lu, H. X. Chen, S. M. Lu and T. D. Liang, Analysis of adverse reactions and plasma concentrations of oral commonly used dose sustained-release theophylline in the elderly, *J. Emerg. Med.*, 2020, **25**(1), 3.
14 S. A. Stanton, J. J. Du, F. Lai, G. Stanton, B. A. Hawkins, J. A. Ong, P. W. Groundwater, J. A. Platts and D. E. Hibbs, Understanding Hygroscopicity of Theophylline *via* a Novel Cocrystal Polymorph: A Charge Density Study, *J. Phys. Chem. A*, 2021, **125**(45), 9736–9756.
15 G. Bolla, B. Sarma and A. K. Nangia, Crystal engineering of pharmaceutical cocrystals in the discovery and development of improved drugs, *Chem. Rev.*, 2022, **122**(13), 11514–11603.

16 M. A. Yousef and V. R. Vangala, Pharmaceutical cocrystals: molecules, crystals, formulations, medicines, *Cryst. Growth Des.*, 2019, **19**(12), 7420–7438.
17 R. Shaikh, R. Singh, G. M. Walker and D. M. Croker, Pharmaceutical Cocrystal Drug Products: An Outlook on Product Development, *Trends Pharmacol. Sci.*, 2018, **39**(12), 1033–1048.
18 N. Qiao, M. Li, W. Schlindwein, N. Malek, A. Davies and G. Trappitt, Pharmaceutical cocrystals: An overview, *Int. J. Pharm.*, 2011, **419**(1–2), 1–11.
19 M. Gryl, S. Cenedese and K. Stadnicka, Crystal Engineering and Charge Density Study of Pharmaceutical Nonlinear Optical Material: Melamine-Barbital Co-Crystal, *J. Phys. Chem. C*, 2014, **119**(1), 590–598.
20 B. Dittrich, Is there a future for topological analysis in experimental charge-density research? Acta Crystallographica Section B Structural Science, *Acta Crystallogr., Sect. B*, 2017, **73**(3), 325–329.
21 W. Kuang, S. Ji, Y. Wei, J. Zhang and P. Lan, A new 1:1 cocrystal of lamotrigine and 1,2,3,6-hydrophthalimide: discovery, characterization, and construction of ternary phase diagrams, *CrystEngComm*, 2020, **22**(15), 2681–2688.
22 G. Kuminek, K. L. Cavanagh, M. F. M. da Piedade and N. Rodríguez-Hornedo, Posaconazole Cocrystal with Superior Solubility and Dissolution Behavior, *Cryst. Growth Des.*, 2019, **19**(11), 6592–6602.
23 J. Wang, X.-L. Dai, T.-B. Lu and J.-M. Chen, Temozolomide–Hesperetin Drug–Drug Cocrystal with Optimized Performance in Stability, Dissolution, and Tabletability, *Cryst. Growth Des.*, 2021, **21**(2), 838–846.
24 D. Bernasconi, S. Bordignon, F. Rossi, E. Priola, C. Nervi, R. Gobetto, D. Voinovich, D. Hasa, N. T. Duong, Y. Nishiyama and M. R. Chierotti, Selective Synthesis of a Salt and a Cocrystal of the Ethionamide–Salicylic Acid System, *Cryst. Growth Des.*, 2019, **20**(2), 906–915.
25 M.-H. Qi, H. Li, B. Zhu, M. Hong and G.-B. Ren, Cocrystals of Oxymatrine: Reducing Hygroscopicity and Affecting the Dissolution Rate, *Cryst. Growth Des.*, 2021, **21**(7), 3874–3888.
26 T. Friščić, L. Fábián, J. C. Burley, D. G. Reid, M. J. Duer and W. Jones, Exploring the relationship between cocrystal stability and symmetry: is Wallach's rule applicable to multi-component solids?, *Chem. Commun.*, 2008, **14**, 1644–1646.
27 H. Liu, H. C. S. Chan, X. Yu, J. Li, J. Li and Z. Zhou, Two Polymorphic Cocrystals of Theophylline with Ferulic Acid, *Cryst. Growth Des.*, 2023, **23**(6), 4448–4459.
28 S. Darwish, J. Zeglinski, G. R. Krishna, R. Shaikh, M. Khraisheh, G. M. Walker and D. M. Croker, A New 1:1 Drug-Drug Cocrystal of Theophylline and Aspirin: Discovery, Characterization, and Construction of Ternary Phase Diagrams, *Cryst. Growth Des.*, 2018, **18**(12), 7526–7532.
29 Z.-L. Wang and L.-H. Wei, Theophylline–2,4-dihydroxybenzoic acid–water (1/1/1), *Acta Crystallogr., Sect. E:Struct. Rep. Online*, 2007, **63**(4), 1681–1682.
30 S. Aitipamula, P. S. Chow and R. B. H. Tan, Trimorphs of a pharmaceutical cocrystal involving two active pharmaceutical ingredients: potential relevance to combination drugs, *CrystEngComm*, 2009, **11**(9), 1823–1827.
31 F. Fischer, M. U. Schmidt, S. Greiser and F. Emmerling, The challenging case of the theophylline–benzamide cocrystal, *Acta Crystallogr., Sect. C: Struct. Chem.*, 2016, **72**(3), 217–224.
32 A. O. L. Évora, R. A. E. Castro, T. M. R. Maria, M. Ramos Silva, J. Canotilho and M. E. S. Eusébio, Lamotrigine: Design and synthesis of new multicomponent solid forms, *Eur. J. Pharm. Sci.*, 2019, **129**, 148–162.
33 P. Sanphui, S. S. Kumar and A. Nangia, Pharmaceutical Cocrystals of Niclosamide, *Cryst. Growth Des.*, 2012, **12**(9), 4588–4599.
34 D. Markad and S. K. Mandal, An exploration into the amide–pseudo amide hydrogen bonding synthon between a new coformer with two primary amide groups and theophylline, *CrystEngComm*, 2017, **19**(47), 7112–7124.
35 A. Delori, P. T. A. Galek, E. Pidcock, M. Patni and W. Jones, Knowledge-based hydrogen bond prediction and the synthesis of salts and cocrystals of the anti-malarial drug pyrimethamine with various drug and GRAS molecules, *CrystEngComm*, 2013, **15**, 15.
36 I. Nugrahani and M. A. Jessica, Amino Acids as the Potential Co-Former for Co-Crystal Development: A Review, *Molecules*, 2021, **26**, 11.
37 Y. Song, L. Y. Wang, F. Liu, Y. T. Li, Z. Y. Wu and W. Yan, Simultaneously enhancing the in vitro/in vivo performances of acetazolamide using proline as a zwitterionic coformer for cocrystallization, *CrystEngComm*, 2019, **21**, 3064–3073.
38 S. J. Dengale, H. Grohganz, T. Rades and K. Löbmann, Recent advances in co-amorphous drug formulations, *Adv. Drug Delivery Rev.*, 2016, **100**, 116–125.
39 K. Löbmann, H. Grohganz, R. Laitinen, C. Strachan and T. Rades, Amino acids as co-amorphous stabilizers for poorly water soluble drugs–Part 1: Preparation, stability and dissolution enhancement, *Eur. J. Pharm. Biopharm.*, 2013, **85**(3), 873–881.
40 I. Nugrahani and M. A. Jessica, Amino acids as the potential co-former for co-crystal development: a review, *Molecules*, 2021, **26**(11), 3279.
41 A. Shete, S. Murthy, S. Korpale, A. Yadav, S. Sajane, S. Sakhare and R. Doijad, Cocrystals of itraconazole with amino acids: Screening, synthesis, solid state characterization, *in vitro* drug release and antifungal activity, *J. Drug Delivery Sci. Technol.*, 2015, **28**, 46–55.
42 D. Rambabu, J. Satyanarayana, V. G. Saraswatula, N. Ravikumar, S. A. Kamalakaran, G. Gopikrishna and K. A. Kumar, Novel cocrystals/molecular salts of mesalamine to be used as improved anti-inflammatory drug, *WIPO Patent*, WO2012090224A1, 2012.
43 A. Wróblewska, J. Śniechowska, S. Kaźmierski, E. Wielgus, G. D. Bujacz, G. Mlostoń, A. Chworos, J. Suwara and M. J. Potrzebowski, Application of 1-hydroxy-4, 5-dimethyl-imidazole 3-oxide as coformer in formation of pharmaceutical cocrystals, *Pharmaceutics*, 2020, **12**(4), 359.

44 J. C. Krantz, J. M. Holbert, H. K. Iwamoto and C. J. Carr, Sodium Theophylline Glycinate, *J. Am. Pharm. Assoc.*, 1947, **36**(8), 248–250.

45 P. Wang, M. Qi, D. Zhong and L. L. Fang, Pharmacokinetics of a new sustained-release formulation of theophylline sodium glycerinate in healthy subjects with a new asymmetric dosage regimen, *Biomed. Chromatogr.*, 2003, **17**(1), 58–61.

46 D.-H. Ngo and T. S. Vo, An Updated Review on Pharmaceutical Properties of Gamma-Aminobutyric Acid, *Molecules*, 2019, **24**, 15.

47 D. T. Plante, J. E. Jensen, L. Schoerning and J. W. Winkelman, Reduced γ-Aminobutyric Acid in Occipital and Anterior Cingulate Cortices in Primary Insomnia: a Link to Major Depressive Disorder?, *Neuropsychopharmacology*, 2012, **37**(6), 1548–1557.

48 R. H. Böger and S. M. Bode-Böger, The Clinical Pharmacology of L-Arginine, *Annu. Rev. Pharmacol.*, 2001, **41**(1), 79–99.

49 H. Tapiero, G. Mathé, P. Couvreur and K. D. I. Tew, Arginine, *Biomed. Pharmacother.*, 2002, **56**(9), 439–445.

50 H. Puschmann, L. J. Bourhis, O. V. Dolomanov, R. J. Gildea and J. A. Howard, OLEX2-a complete package for molecular crystallography, *Acta Crystallogr., Sect. A*, 2011, **67**, C593.

51 H. Puschmann and O. Dolomanov, OLEX2: TEACHING NEW SOFTWARE OLD AND NEW TRICKS, *Acta Crystallogr., Sect. A*, 2019, **75**, e766.

52 F. Kleemiss, O. V. Dolomanov, M. Bodensteiner, N. Peyerimhoff, L. Midgley, L. J. Bourhis, A. Genoni, L. A. Malaspina, D. Jayatilaka, J. L. Spencer, F. White, B. Grundkötter-Stock, S. Steinhauer, D. Lentz, H. Puschmann and S. Grabowsky, Accurate crystal structures and chemical properties from NoSpherA2, *Chem. Sci.*, 2021, **12**(5), 1675–1692.

53 L. Midgley, L. J. Bourhis, O. V. Dolomanov, S. Grabowsky, F. Kleemiss, H. Puschmann and N. Peyerimhoff, Vanishing of the atomic form factor derivatives in non-spherical structural refinement–a key approximation scrutinized in the case of Hirshfeld atom refinement, *Acta Crystallogr., Sect. A:Found. Adv.*, 2021, **77**(6), 519–533.

54 J. Lübben, C. M. Wandtke, C. B. Hübschle, M. Ruf, G. M. Sheldrick and B. Dittrich, Aspherical scattering factors for SHELXL–model, implementation and application, *Acta Crystallogr., Sect. A:Found. Crystallogr.*, 2019, **75**(1), 50–62.

55 L. J. Barbour, X-Seed—A software tool for supramolecular crystallography, *J. Supramol. Chem.*, 2001, **1**(4–6), 189–191.

56 C. F. Macrae, I. Sovago, S. J. Cottrell, P. T. Galek, P. McCabe, E. Pidcock, M. Platings, G. P. Shields, J. S. Stevens and M. Towler, Mercury 4.0: From visualization to analysis, design and prediction, *J. Appl. Crystallogr.*, 2020, **53**(1), 226–235.

57 S. Emami, R. Ghafari and E. Manafzadeh, Solid-State Interaction of Pharmaceutical Cocrystals with Water Vapor, *Cryst. Growth Des.*, 2021, **21**(8), 4805–4820.

58 M. Humar, R. Repič, D. Kržišnik, B. Lesar, R. Cerc Korošec, C. Brischke, L. Emmerich and G. Rep, Quality Control of Thermally Modified Timber Using Dynamic Vapor Sorption (DVS) Analysis, *Forests*, 2020, **11**, 6.

59 R. F. W. Bader, Atoms in molecules, *Acc. Chem. Res.*, 1985, **18**(1), 9–15.

60 M. Frisch, G. Trucks, H. Schlegel, G. Scuseria, M. Robb, J. Cheeseman, G. Scalmani, V. Barone, G. Petersson and H. Nakatsuji, *Gaussian 16*, Revision A. 03, Gaussian, Inc., Wallingford CT, G16 A.03, 2016.

61 T. Lu and F. Chen, Multiwfn: A multifunctional wavefunction analyzer, *J. Comput. Chem.*, 2012, **33**(5), 580–592.

62 P. R. Spackman, M. J. Turner, J. J. McKinnon, S. K. Wolff, D. J. Grimwood, D. Jayatilaka and M. A. Spackman, CrystalExplorer: A program for Hirshfeld surface analysis, visualization and quantitative analysis of molecular crystals, *J. Appl. Crystallogr.*, 2021, **54**(3), 1006–1011.

63 W. M. Latimer and W. H. Rodebush, Polarity and ionization from the standpoint of the Lewis theory of valence, *J. Am. Chem. Soc.*, 1920, **42**(7), 1419–1433.

64 Z. S. Derewenda, On the centennials of the discoveries of the hydrogen bond and the structure of the water molecule: the short life and work of Eustace Jean Cuy (1897–1925), *Acta Crystallogr., Sect. A:Found. Adv.*, 2021, **77**(5), 362–378.

65 H. Yu, B. Zhang, M. Liu, W. Xing, K. Hu, S. Yang, G. He, N. Gong, G. Du and Y. Lu, Design, Preparation, Characterization and Evaluation of Five Cocrystal Hydrates of Fluconazole with Hydroxybenzoic Acids, *Pharmaceutics*, 2022, **14**, 11.

66 S. Aitipamula, P. S. Chow and R. B. H. Tan, Co-crystals of caffeine and piracetam with 4-hydroxybenzoic acid: Unravelling the hidden hydrates of 1: 1 co-crystal, *CrystEngComm*, 2012, **14**, 7.

67 S. Emamian, T. Lu, H. Kruse and H. Emamian, Exploring Nature and Predicting Strength of Hydrogen Bonds: A Correlation Analysis Between Atoms-in-Molecules Descriptors, Binding Energies, and Energy Components of Symmetry-Adapted Perturbation Theory, *J. Comput. Chem.*, 2019, **40**(32), 2868–2881.

68 S. Alam, S. Patel and A. K. Bansal, Effect of sample preparation method on quantification of polymorphs using PXRD, *Pharm. Dev. Technol.*, 2009, **15**(5), 452–459.

69 J. D. Menczel, L. Judovits and R. B. Prime, Differential scanning calorimetry (DSC), *Thermal Analysis of Polymers: Fundamentals and Applications*, 2009, pp. 7–239.

70 S. Ishihara, Y. Hattori and M. Otsuka, MCR-ALS analysis of IR spectroscopy and XRD for the investigation of ibuprofen - nicotinamide cocrystal formation, *Spectrochim. Acta, Part A*, 2019, **221**, 117142.

71 A. W. Newman, S. M. Reutzel-Edens and G. Zografi, Characterization of the hygroscopic properties of active pharmaceutical ingredients, *J. Pharm. Sci.*, 2008, **97**(3), 1047–1059.

72 C. Ahlneck and G. Zografi, The molecular basis of moisture effects on the physical and chemical stability of drugs in the solid state, *Int. J. Pharm.*, 1990, **62**(2–3), 87–95.

73 D. P. Kale, B. Ugale and C. M. Nagaraja, Molecular basis of water sorption behavior of rivaroxaban-malonic acid cocrystal, *Mol. Pharm.*, 2019, **16**(7), 2980–2991.
74 A. S. Mitchell and M. A. Spackman, Molecular surfaces from the promolecule: A comparison with Hartree-Fockab initio electron density surfaces, *J. Comput. Chem.*, 2000, **21**(11), 933–942.
75 J. Varshosaz, Biopharmaceutical characterization of oral theophylline and aminophylline tablets. Quantitative correlation between dissolution and bioavailability studies, *Eur. J. Pharm. Biopharm.*, 2000, **50**(2), 301–306.
76 D. D. Bavishi and C. H. Borkhataria, Spring and parachute: How cocrystals enhance solubility, *Prog. Cryst. Growth Charact. Mater.*, 2016, **62**(3), 1–8.